Electronic Supplementary Material (ESI) for Green Chemistry.

Electronic Supporting Information

Constructing single Cu-N_3 sites for CO_2 electrochemical reduction over a wide potential range

Jiaqi Feng,[a,b] Lirong Zheng,[c] Chongyang Jiang,[a,b] Zhipeng Chen,[d] Lei Liu,[a] Shaojuan Zeng,[a] Lu Bai,[a] Suojiang Zhang*[a,b] and Xiangping Zhang*[a,b]

[a] Beijing Key Laboratory of Ionic Liquids Clean Process, State Key Laboratory of Multiphase Complex Systems, Institute of Process Engineering, Chinese Academy of Sciences, Beijing 100190, China.

[b] College of Chemical Engineering, University of Chinese Academy of Science, Beijing 100190, China.

[c] Beijing Synchrotron Radiation Facility (BSRF), Institute of High Energy Physics, Chinese Academy of Sciences, Beijing 100190, China.

[d] CAS Key Laboratory of Bio-based Materials, Qingdao Institute of Bioenergy and Bioprocess Technology, Chinese Academy of Sciences, Qingdao 266101, China

1. Experimental section

Materials. 1-butyl-3-methylimidazolium tetrachlorocuprate ($[Bmim]_2[CuCl_4]$) was synthesized as reported in our prior work.[1] 1-butyl-2,3-dimethylimidazolium tetrafluoroborate ($[BMmim][BF_4]$, purity>99%) and 1-butyl-3-methylimidazolium chloride ([Bmim][Cl]) were purchased from Shanghai chengjie Co., Ltd. Multi-walled carbon nanotubes (MWCNTs) were provided by XFNANO. Carbon cloth (HCP331P, 19×19 cm), Nafion N-117 membrane (0.180 mm thick, ≥0.90 meg/g exchange capacity) and Nafion D-521 dispersion (5 % w/w in water and 1-propanol, ≥ 0.92 meg/g exchange capacity) were purchased from Shanghai Hesen electric Co., Ltd. potassium bicarbonate ($KHCO_3$) was purchased from Shanghai Aladdin Biochemical Tech. Co., Ltd. All the aqueous solutions were prepared by Milli Q water (18.2 MΩ cm, 298 K).

Synthesis of Cu-N-CNT. The surface modification of CNTs was done according to our prior work[2]. 50 mg of treated CNTs and 45 mg of $[Bmim]_2[CuCl_4]$ were sonicated in 100 mL water and then stirred at 60℃ for 8 h. The mixture was dried up using lyophilization and annealed at 600℃ for 1 h under nitrogen atmosphere. To obtain the final product of Cu-N-CNT, the as-annealed powders were further treated with 1 M HCl and washed with water several times and finally vacuum dried.

Synthesis of N-CNT. N-CNT was prepared by the same procedure as Cu-N-CNT except for replacing $[Bmim]_2[CuCl_4]$ as 32.5 mg [Bmim][Cl].

Synthesis of Cu_xO_y/CNT. Cu_xO_y/CNT was prepared by the same procedure as Cu-N-CNT except for replacing $[Bmim]_2[CuCl_4]$ as 12.5 mg $CuCl_2$ and the omissions of HCl treatment.

Synthesis of Cu-N-CNT-S. Cu-N-CNT-S was prepared by the same procedure as Cu-N-CNT except for replacing $[Bmim]_2[CuCl_4]$ as 32.5 mg [Bmim][Cl] and 12.5 mg $CuCl_2$.

Characterization. Scanning electronic microscopy (SEM) was performed using a Hitachi SU8020 electron microscopy operated at 5 kV. Transmission electron microscopy (TEM) was performed on JEOL JEM-2100 system and the high-angle annular dark-field scanning transmission electron microscopy (HAADF-STEM) characterization and corresponding energy-dispersive spectroscopy (EDS) were conducted on a JEOL JEM-ARF200F TEM/STEM with a spherical aberration corrector. Powder X-ray diffraction (XRD) measurements were recorded with Rigaku Smartlab diffractometer with Cu Kα radiation (λ = 1.5418 Å) operated at 45 kV and an emission of 50 mA. The scattering range of 2θ was from 5 to 90° with scanning rate of 15° min^{-1}. The N_2 adsorption-desorption isotherms of catalysis was recorded at 77 K on a Quantachrome Instrument NOVA 2000 and specific surface area was determined by Brunauer-Emmett-Teller (BET) method. The X-ray photoelectron spectroscopy (XPS) was determined by a Thermo Fisher Scientific ESCALAB 250Xi using Al Kα (1486.6 eV) X-ray source under a pressure of 3×10^{-7} mbar and binding energy were referenced to the C 1s peak at 284.8 eV. The X-ray absorption find structure spectra (Cu K-edge) were collected at 1W1B station in Beijing Synchrotron Radiation Facility (BSRF). The storage rings of BSRF were operated at 2.5 GeV with a maximum current of 250 mA. Using Si (111) double-crystal monochromator, the data collection was carried out in fluorescence mode using ionization chamber. All spectra were collected in ambient conditions, and data of XAFS were processed according to the standard procedures using the ATHENA module implemented in the IFEFFIT software packages. The k^3 - weighted EXAFS spectra were obtained by subtracting the post-edge background from the overall absorption and then normalizing with respect to the edge-jump step. Subsequently, k^3 - weighted $\chi(k)$ data of Cu K - edge were Fourier transformed to real (R) space using a hanging windows (dk = 1.0 Å^{-1}) to separate the EXAFS contributions from different coordination shells. To obtain the quantitative structural parameters around central atoms, least-squares curve parameter fitting was performed using the ARTEMIS module of IFEFFIT software packages[3-5].

Preparation of working electrodes. The catalyst ink was prepared by ultrasonic of 1.5 mg catalyst powder suspended in 240 μL of isopropanol and

40 μL of Nafion D-521 to form a homogeneous ink. For experiments in H-typed cell, the catalyst ink was uniformly spread on carbon paper (HCP331P) of 1 × 1 cm^2 in area. For experiments in flow cell, the catalyst ink was uniformly spread on carbon paper (YLS-30T) of 0.5 × 2 cm^2 in area.

Electrochemical test. The electrochemical measurements were controlled with a CHI 660E potentiostat. All potentials were measured against Ag / AgCl (aqueous electrolyte, 3.0 M KCl) or Ag / Ag^+ (ionic liquid electrolyte) reference electrode. The Ag / AgCl reference electrode was converted to the RHE reference scale using:

$$E\ (vs.\ \mathrm{RHE}) = E\ (vs.\ \mathrm{Ag\ /\ AgCl}) + 0.21 + (0.0591 \times \mathrm{pH})$$

For experiments in H-typed cell, the two compartments were separated by a proton exchange membrane. Platinum gauze was used as the counter electrode. The working and reference electrodes were placed in the cathode chamber with 0.5 M $KHCO_3$ solution or $[BMmim][BF_4]/CH_3CN/H_2O$ mixture solution containing 30 wt% $[BMmim][BF_4]$, 65 wt% CH_3CN, and 5 wt% H_2O as electrolyte, while the counter electrode was placed in the anode chamber with 0.1 M H_2SO_4 solution as electrolyte. Before the experiment, the electrolyte in cathode chamber was bubbled with N_2 or CO_2 (30 mL min^{-1}) for at least 30 min to form N_2 or CO_2 saturated solution.

For experiments in flow cell, the two compartments were separated by an anion exchange membrane. Platinum foil was used as the counter electrode. The CO_2 flow through cathode compartment was maintained at 45 mL min^{-1} and the electrolyte 1 M KOH was maintained at a rate of 20 mL min^{-1} using peristaltic pump.

Computational Details for Calculations. The DFT calculations were performed by using the Vienna ab initio Simulation Package (VASP)[6]. The projector-augmented wave (PAW) method and PBE potential for the exchange correlation functional were used[7]. The Kohn-Sham wave functions were expanded in a plane wave basis set with a cutoff energy of 500 eV. The DFT+D3 method developed by Grimme was employed to treat the Vander Waals interactions[8]. A 4×4×1 Monkhorst-Pack k-point sampling of the Brillouin zone was adopted for the structure optimization and an 8×8×1 k-point sampling was used for the single-point energy and electronic structure calculations. For the structure optimization, the total energy and force convergences were set to be smaller than 10^{-6} eV and 0.01 eV $Å^{-1}$. We employed a graphene supercell with surface periodicity of 5 × 5 including 50 atoms as a basis to construct the C/Cu-Nx moieties. A vacuum region of 15 Å was created to ensure negligible interaction between mirror images. We corrected the free energy of each structure at 289.15 K by the using the Vaspkit.

The CO_2RR occur via the following steps:

$$CO_2 + * \rightarrow *CO_2$$

$$*CO_2 + H+ +e- \rightarrow *COOH$$

$$*COOH + H+ +e- \rightarrow *CO + H_2O$$

$$*CO \rightarrow CO + *$$

where * represents the preferable adsorption site for intermediates.

2. Supplementary Figures and Tables

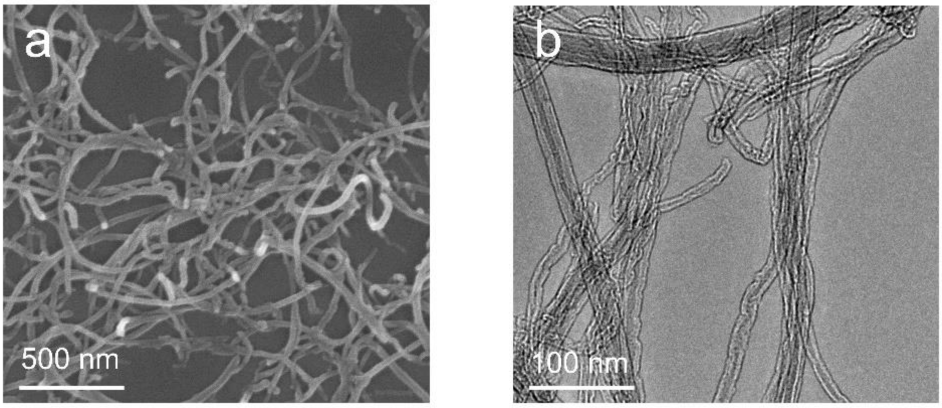

Fig. S1. (a) SEM image and (b) TEM image of N-CNT.

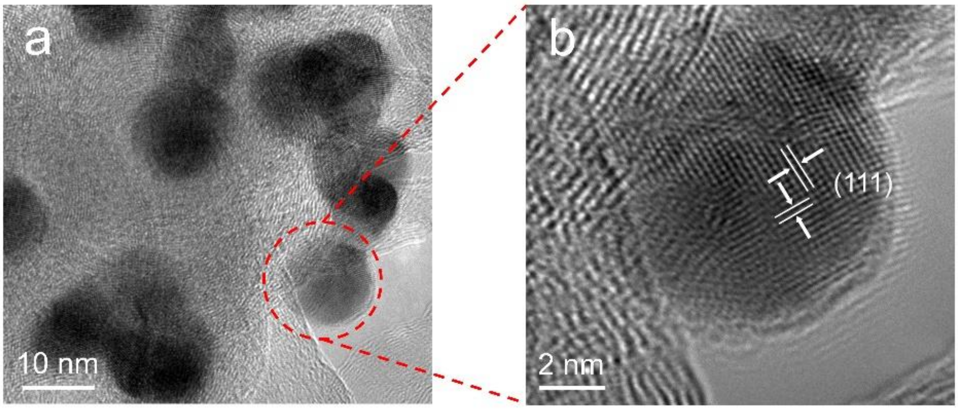

Fig. S2 (a) Large-field view and (b) magnified view of TEM images of Cu_xO_y/CNT.

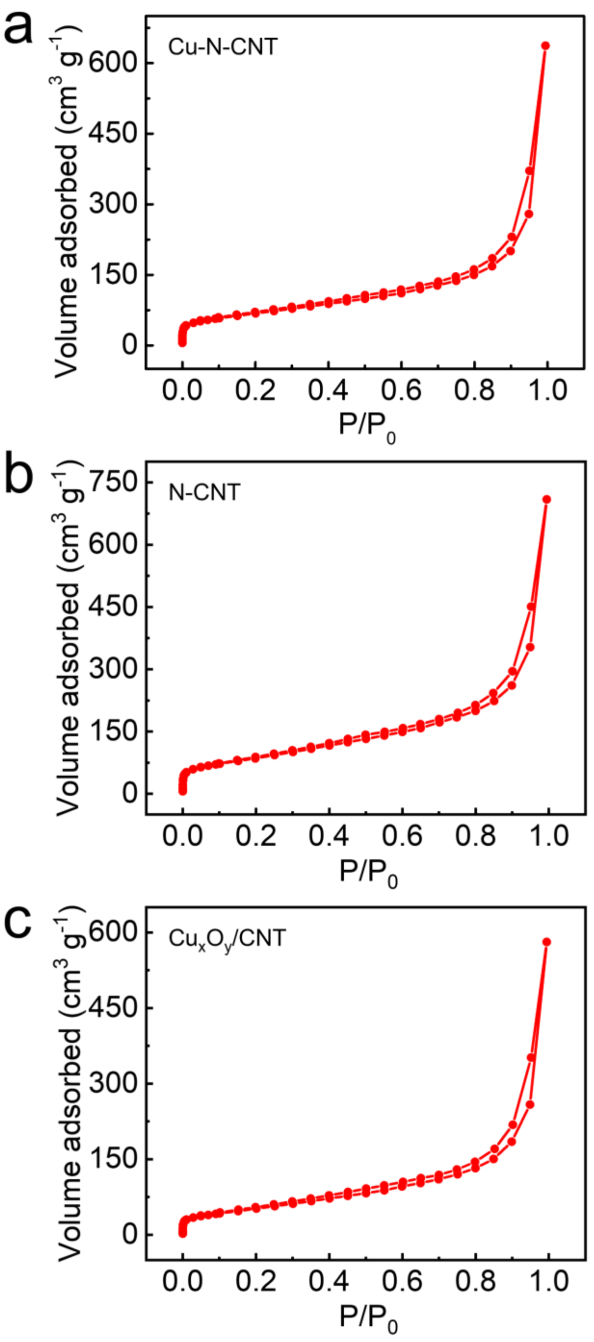

Fig. S3. The N_2 adsorption-desorption isotherms of (a) Cu-N-CNT, (b) N-CNT and (c) Cu_xO_y/CNT.

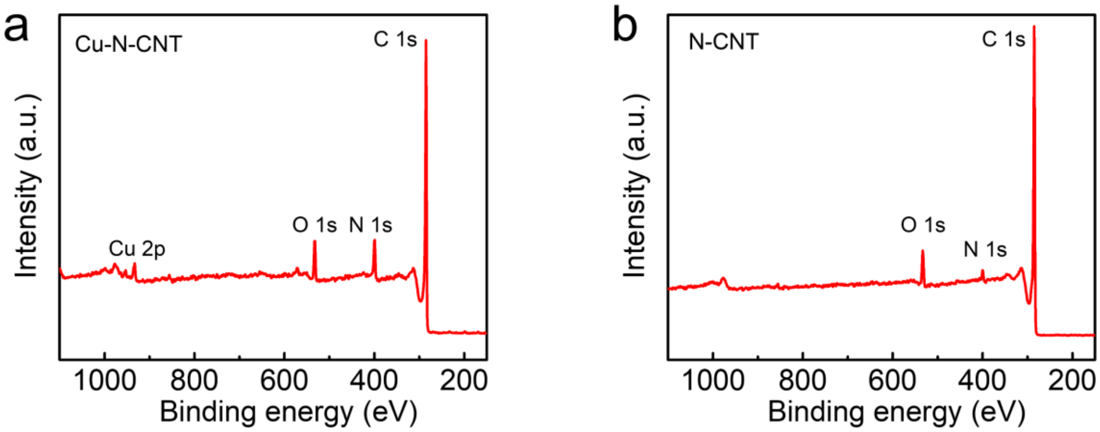

Fig. S4. Full XPS spectra of (a) Cu-N-CNT and (b) N-CNT.

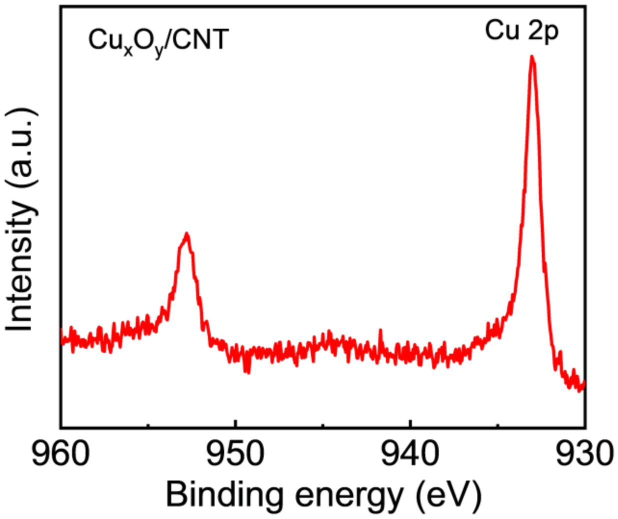

Fig. S5. The high-resolution Cu 2p XPS spectra of Cu$_x$O$_y$/CNT.

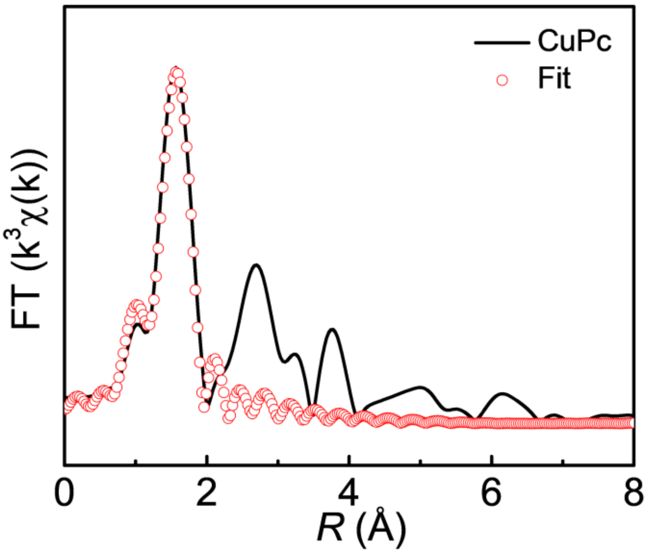

Fig. S6. EXAFS fitting curves of the CuPc in R space.

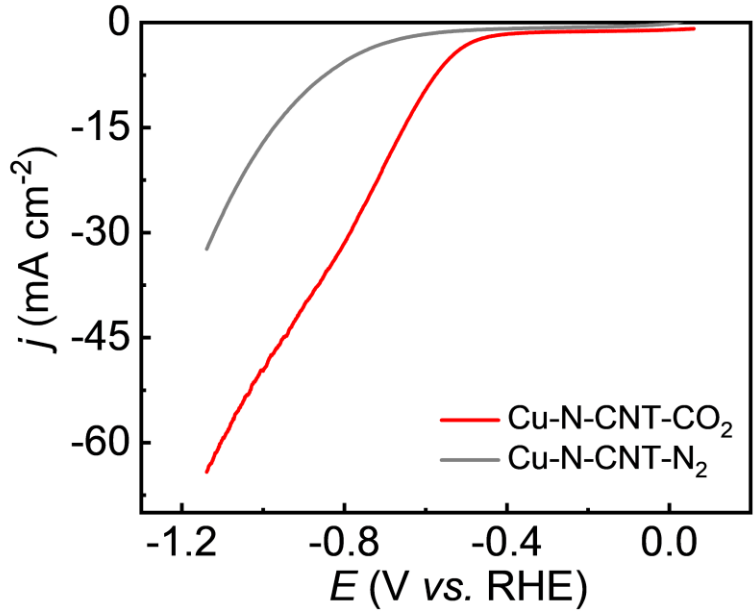

Fig. S7. LSV curves for Cu-N-CNT in CO_2- and N_2-saturated 0.5 mol L^{-1} $KHCO_3$ solution.

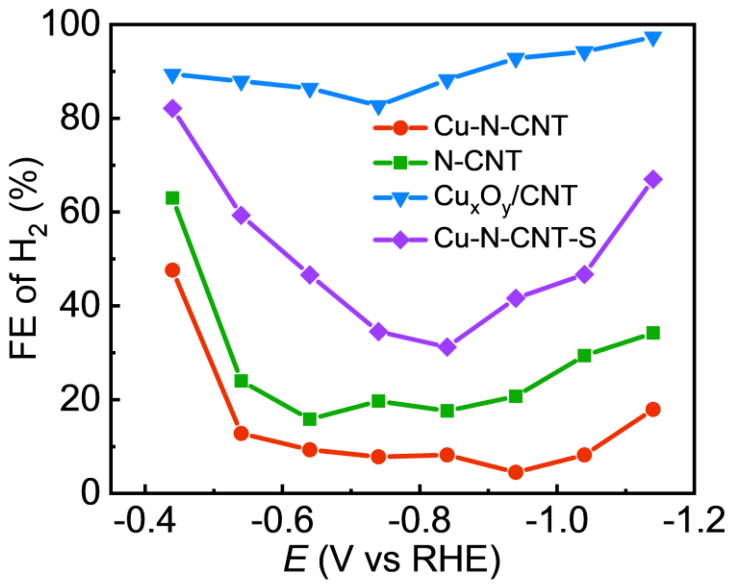

Fig. S8. The H_2 FE of Cu-N-CNT, N-CNT, Cu_xO_y/CNT and Cu-N-CNT-S at different applied potentials in CO_2-saturated $KHCO_3$ electrolyte

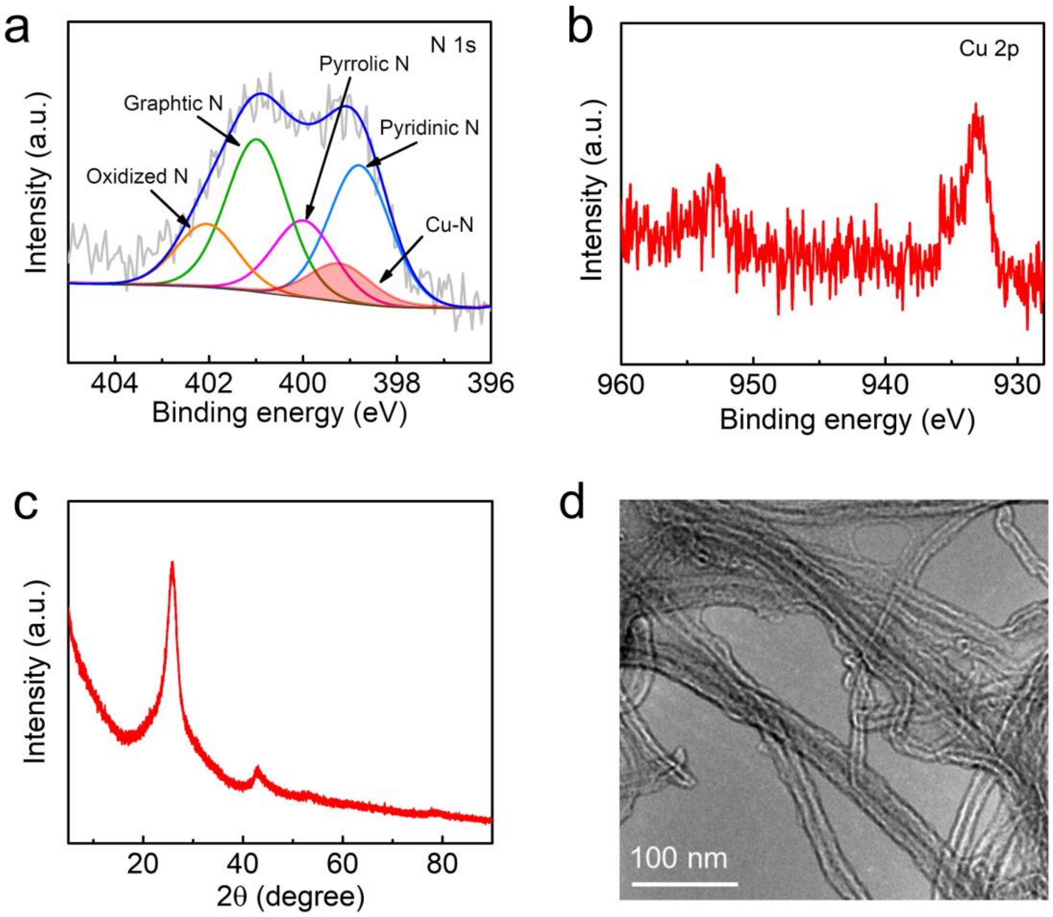

Fig. S9. The (a) high-resolution N 1s, (b) Cu 2p XPS spectra, (c) XRD pattern, and (d) TEM image of Cu-N-CNT after long-term electrolysis.

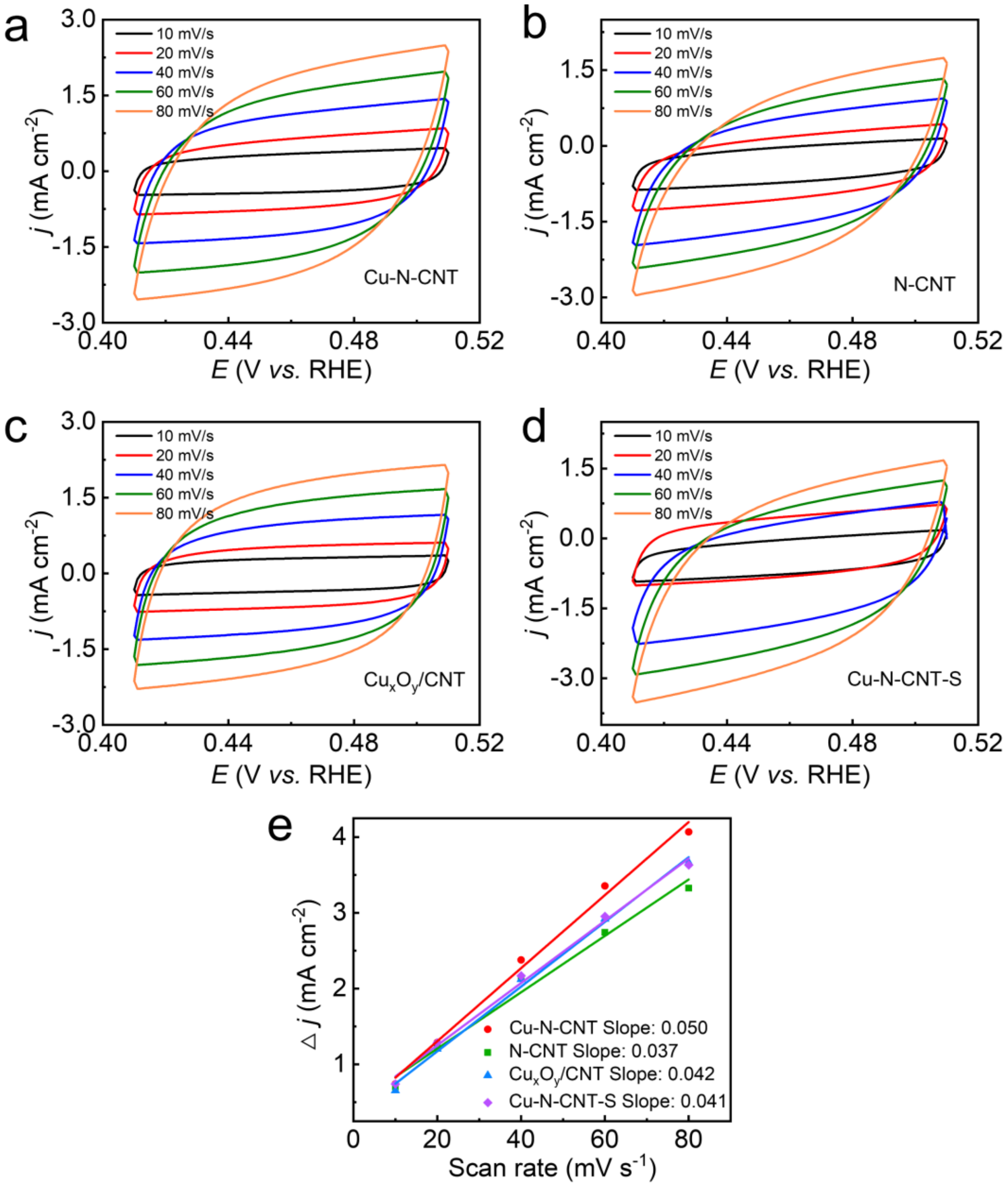

Fig. S10. Cyclic voltammograms at the range of 0.5 V to 0.6 V with different scan rates for (a) Cu-N-CNT, (b) N-CNT, (c) Cu_xO_y/CNT and (d) Cu-N-CNT-S. (e) Charging current density differences plotted against scan rate.

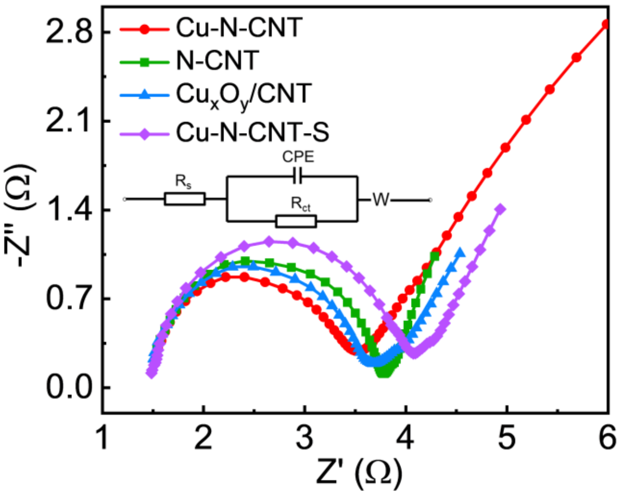

Fig. S11. EIS spectra of Cu-N-CNT, N-CNT, Cu$_x$O$_y$/CNT and Cu-N-CNT-S.

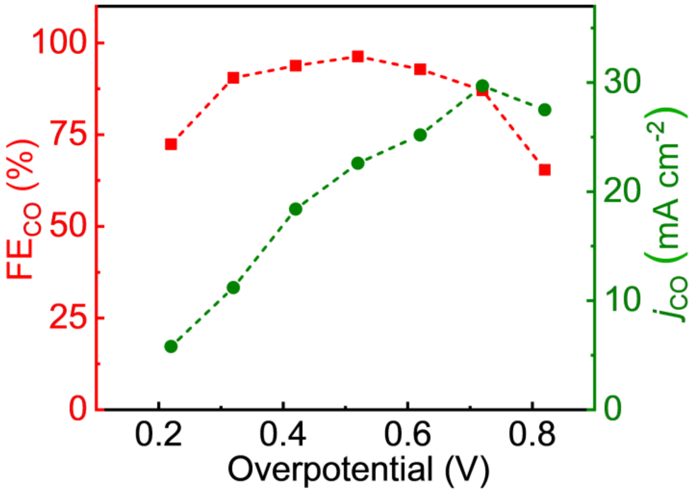

Fig. S12. CO FE and partial CO current density of Cu-N-CNT at different applied potentials in CO_2-saturated [BMmim][BF_4]/CH_3CN-H_2O electrolyte.

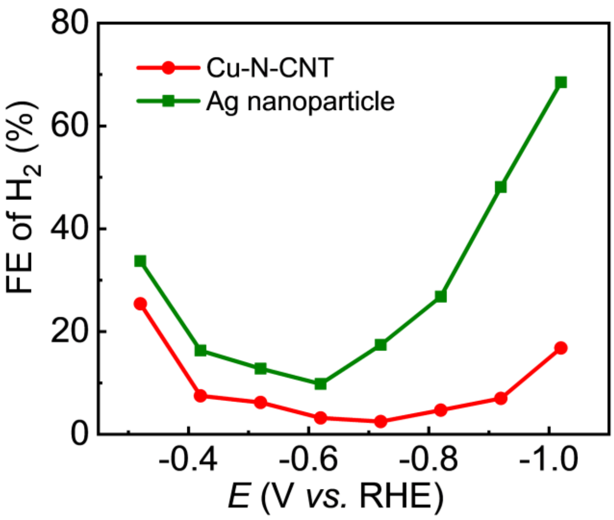

Fig. S13. The H_2 FE of Cu-N-CNT and Ag nanoparticles at different applied potentials in flow cell.

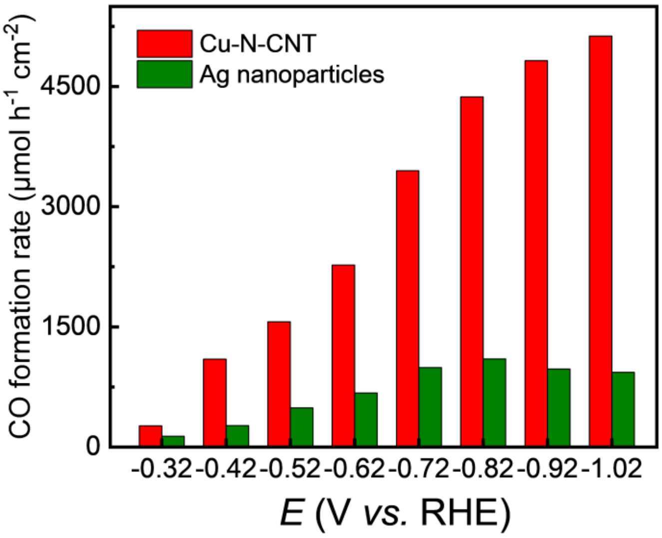

Fig. S14. The CO formation rate of Cu-N-CNT and Ag nanoparticles at different applied potentials in flow cell.

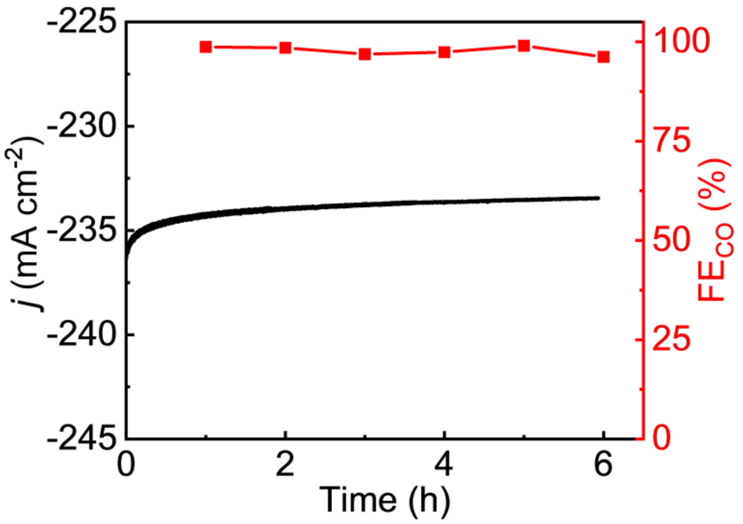

Fig. S15. The CO FE and current density of the Cu-N-CNT operated at -0.82 V for 6 h in flow cell

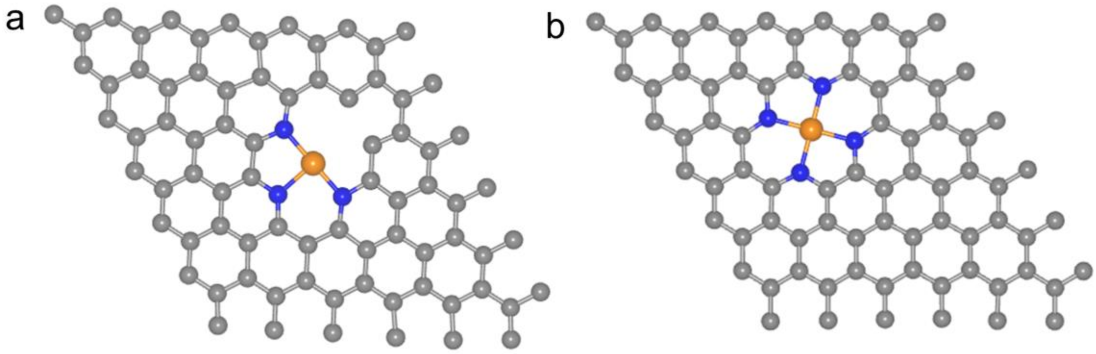

Fig. S16. The structures of the (a) Cu-N_3-C and (b) Cu-N_4-C

Table S1. EXAFS fitting parameters at the Cu K-edge for various samples

Sample	Shell	N [a]	R (Å) [b]	σ^2 (Å^2·10^{-3}) [c]	ΔE_0 (eV) [d]	*R* factor (%)
Cu-N-CNT	Cu-N	2.8	2.02	7.9	8.6	0.9
	Cu-Cu	1.5	2.48	12.1	-7.3	
CuPc	Cu-N	4	1.95	3.0	6.5	0.9

[a] *N*: coordination numbers; [b] *R*: bond distance; [c] σ^2: Debye-Waller factors; [d] ΔE_0: the inner potential correction. *R* factor: goodness of fit. S_0^2 were set as 0.86/0.90 for Cu-N/Cu-Cu, which were obtained from the experimental EXAFS fit of reference CuPc/Cu foil by fixing CN as the known crystallographic value and was fixed to all the samples.

Table S2. The fitting values of EIS equivalent circuit

Electrocatalysts	R_s (Ω)	R_{ct} (Ω)
Cu-N-CNT	1.5	1.8
N-CNT	1.5	2.1
Cu_xO_y/CNT	1.5	2.0
Cu-N-CNT-S	1.5	2.3

Table S3. Performance comparison of various reported CO_2RR electrocatalysts in H-type cell and flow cell

Catalyst	Electrolyte	*E* (V vs. RHE)	FE_{CO} (%)	j_{CO} (mA cm^{-2})	Cell type	Ref.
CoPc-CN	0.1 M $KHCO_3$	-0.63	98	14.7	H cell	[9]
CoPpc	0.5 M $NaHCO_3$	-0.61	90	18	H cell	[10]
Cu SAs/NC	0.1 M $KHCO_3$	-0.70	92	3.47	H cell	[11]

Cu-N$_2$/GN	0.1 M KHCO$_3$	-0.50	81	2.1	H cell	12
Cu-N$_4$-C	0.1 M KHCO$_3$	-0.74	62	0.74	H cell	13
Cu$_{0.5}$NC	0.1 M CsHCO$_3$	-0.60	75	1.88	H cell	14
Cu-APC	0.2 M NaHCO$_3$	-0.78	92	8.6	H cell	15
Cu-N-CNT	0.5 M KHCO$_3$	-0.74	95.7	18.7	H cell	This work
	1 M KOH	-0.82	98.7	234.3	Flow cell	
Cu-N$_4$-C/1100	0.5 M KHCO$_3$	-0.67	93	6.7	GDE [a]	16
CoPc2	0.5 M NaHCO$_3$	-0.676	93	18.1	H cell	17
	1 M KOH	-0.92	94	165	Flow cell	
CoPc-CN	1 M KOH	-0.66	94	31	Flow cell	18
Fe^{3+}-N-C	0.5 M KHCO$_3$	-0.45	~92	94	Flow cell	19
CdS NNs	5 M KOH	-1.2	95.5	212	Flow cell	20
Ni@NCH-1000	0.5 M KHCO$_3$	3 [b]	~90	~100	Flow cell	21
NiPc-Me-MDE	1 M KHCO$_3$	-0.61	99.6	150	Flow cell	22
		-0.69	99.1	400		
Ni-N-C	1 M KHCO$_3$	-0.86	85	~200	Flow cell	23
NiSA/PCFM	0.5 M KHCO$_3$	-1.0	88	308.4	Flow cell	24
Ni-N@IL	1 M KHCO$_3$	-0.65	99.4	103	Flow cell	25
CD-Ag/PTFE	1 M KOH	-0.78	~92	150	Flow cell	26

[a] The electrochemical hydrogen pump reactor equipped with a gas diffusion electrode

[b] Cell potential

3. References

1. Q. Wang, Y. Geng, X. Lu and S. Zhang, *ACS Sustainable Chem. Eng.*, 2015, **3**, 340-348.
2. J. Feng, H. Gao, L. Zheng, Z. Chen, S. Zeng, C. Jiang, H. Dong, L. Liu, S. Zhang and X. Zhang, *Nat. Commun.*, 2020, **11**, 4341.
3. B. Ravel and M. Newville, *J. Synchrotron. Radiat.*, 2005, **12**, 537-541.
4. J. J. Rehr and R. C. Albers, *Rev. Mod. Phys.*, 2000, **72**, 621-654.
5. D. Koningsberger and R. Prins, *(Wiley, New York, 1988)*, 1988.
6. G. Kresse and J. Furthmuller, *Phys. Rev. B*, 1996, **54**, 11169-11186.
7. P. E. Blochl, *Phys. Rev. B*, 1994, **50**, 17953-17979.
8. M. Homberg and M. Muller, *J. Chem. Phys.*, 2010, **132**, 155104.
9. X. Zhang, Z. Wu, X. Zhang, L. Li, Y. Li, H. Xu, X. Li, X. Yu, Z. Zhang, Y. Liang and H. Wang, *Nat. Commun.*, 2017, **8**, 14675.
10. N. Han, Y. Wang, L. Ma, J. Wen, J. Li, H. Zheng, K. Nie, X. Wang, F. Zhao, Y. Li, J. Fan, J. Zhong, T. Wu, D. J. Miller, J. Lu, S.-T. Lee and Y. Li, *Chem*, 2017, **3**, 652-664.
11. F. Yang, X. Mao, M. Ma, C. Jiang, P. Zhang, J. Wang, Q. Deng, Z. Zeng and S. Deng, *Carbon*, 2020, **168**, 528-535.
12. W. Zheng, J. Yang, H. Chen, Y. Hou, Q. Wang, M. Gu, F. He, Y. Xia, Z. Xia, Z. Li, B. Yang, L. Lei, C. Yuan, Q. He, M. Qiu and X. Feng, *Adv. Funct. Mater.*, 2019, **30**, 1907658.
13. J. Wen, A. Bagger, G.-P. Hao, A. S. Varela, I. Sinev, V. Bon, B. Roldan Cuenya, S. Kaskel, J. Rossmeisl and P. Strasser, *Nat. Commun.*, 2017, **8**, 944.
14. M. Fontecave, D. Karapinar, N. H. Tran, N. Ranjbar Sahraie, J. Li, N. Touati, S. Zanna, D. Taverna, L. H. Galvao Tizei, A. Zitolo, F. Jaouen, V. Mougel and D. Wakerley, *Angew. Chem. Int. Ed.*, 2019, **58**, 15098-15103.
15. J. Jiao, R. Lin, S. Liu, W. C. Cheong, C. Zhang, Z. Chen, Y. Pan, J. Tang, K. Wu, S. F. Hung, H. M. Chen, L. Zheng, Q. Lu, X. Yang, B. Xu, H. Xiao, J. Li, D. Wang, Q. Peng, C. Chen and Y. Li, *Nat. Chem.*, 2019, **11**, 222-228.
16. H. Cheng, X. Wu, X. Li, X. Nie, S. Fan, M. Feng, Z. Fan, M. Tan, Y. Chen and G. He, *Chem. Eng. J.*, 2021, **407**, 126842.
17. M. Wang, K. Torbensen, D. Salvatore, S. Ren, D. Joulie, F. Dumoulin, D. Mendoza, B. Lassalle-Kaiser, U. Isci, C. P. Berlinguette and M. Robert, *Nat. Commun.*, 2019, **10**, 3602.
18. X. Lu, Y. Wu, X. Yuan, L. Huang, Z. Wu, J. Xuan, Y. Wang and H. Wang, *ACS Energy Lett.*, 2018, **3**, 2527-2532.
19. J. Gu, C.-S. Hsu, L. Bai, H. M. Chen and X. Hu, *Science*, 2019, **364**, 1091-1094.
20. F. Y. Gao, S. J. Hu, X. L. Zhang, Y. R. Zheng, H. J. Wang, Z. Z. Niu, P. P. Yang, R. C. Bao, T. Ma, Z. Dang, Y. Guan, X. S. Zheng, X. Zheng, J. F. Zhu, M. R. Gao and S. H. Yu, *Angew. Chem. Int. Ed.*, 2020, **59**, 8706-8712.
21. R. Daiyan, X. Zhu, Z. Tong, L. Gong, A. Razmjou, R.-S. Liu, Z. Xia, X. Lu, L. Dai and R. Amal, *Nano Energy*, 2020, **78**, 105213.
22. X. Zhang, Y. Wang, M. Gu, M. Y. Wang, Z. S. Zhang, W. Y. Pan, Z. Jiang, H. Z. Zheng, M. Lucero, H. L. Wang, G. E. Sterbinsky, Q. Ma, Y. G. Wang, Z. X. Feng, J. Li, H. J. Dai and Y. Y. Liang, *Nat. Energy*, 2020, **5**, 684-692.
23. T. Möller, W. Ju, A. Bagger, X. Wang, F. Luo, T. Ngo Thanh, A. S. Varela, J. Rossmeisl and P. Strasser, *Energ. Environ. Sci.*, 2019, **12**, 640-647.
24. H. Yang, Q. Lin, C. Zhang, X. Yu, Z. Cheng, G. Li, Q. Hu, X. Ren, Q. Zhang, J. Liu and C.

He, *Nat. Commun.*, 2020, **11**, 593.

25. W. Ren, X. Tan, X. Chen, G. Zhang, K. Zhao, W. Yang, C. Jia, Y. Zhao, S. C. Smith and C. Zhao, *ACS Catal.*, 2020, **10**, 13171-13178.
26. C.-T. Dinh, F. P. García de Arquer, D. Sinton and E. H. Sargent, *ACS Energy Lett.*, 2018, **3**, 2835-2840.